Bimetallic Fe–Ni Cluster Alloys: Stability of Core(Fe)–Shell(Ni) Arrays and Their Role Played in the Structure and Magnetic Behavior

ARTICLE *in* THE JOURNAL OF PHYSICAL CHEMISTRY C · APRIL 2008

Impact Factor: 4.77 · DOI: 10.1021/jp7114065

2 AUTHORS:

R. A. Guirado-Lopez
Universidad Autónoma de San Luis Potosí
57 PUBLICATIONS **687** CITATIONS
SEE PROFILE

F. Aguilera-Granja
Universidad Autónoma de San Luis Potosí
150 PUBLICATIONS **1,373** CITATIONS
SEE PROFILE

Bimetallic Fe−Ni Cluster Alloys: Stability of Core(Fe)−Shell(Ni) Arrays and Their Role Played in the Structure and Magnetic Behavior

R. A. Guirado-López* and F. Aguilera-Granja

Instituto de Física "Manuel Sandoval Vallarta", Universidad Autónoma de San Luis Potosí, Alvaro Obregón 64, 78000 San Luis Potosí, México

Received: December 3, 2007; In Final Form: February 25, 2008

We present density functional theory as well as tight-binding calculations to analyze the stability and magnetic properties of small fcc and polyicosahedral Fe−Ni cluster alloys having different compositions and chemical orderings. In agreement with the gas-phase experiments of Parks et al. (*Chem. Phys.* **2000**, *262*, 151), we obtain in all our considered alloys that iron atoms prefer to accumulate in the core region of the structures leading to the formation of highly stable core(Fe)−shell(Ni) arrays. We found that the low energy atomic configurations of our fcc Fe−Ni clusters strongly depend on the chemical order within the structures. Interestingly, fcc particles with Fe-rich core regions are characterized by unusual and considerably expanded Fe−Fe bond lengths (∼2.7 Å), a result that induces a highly nonuniform relaxation profile in which both sizable expansions and contractions of the interatomic distance between neighboring atoms can be obtained. In contrast, disordered alloys and core(Ni)−shell(Fe) arrays are characterized by Fe−Ni bond lengths of ∼2.5 Å, being of the order of the arithmetic weighted average of the Fe−Fe and Ni−Ni pairs. A common feature of our results is that all our considered Fe−Ni clusters exhibit high-spin ground states (larger than the corresponding bulk alloy values for the same composition); however, we have found that iron clustering within the particles, the presence of chemisorbed hydrogens on the surface, as well as the existence of antiferromagnetic order in the iron-rich regions could lead to a sizable quenching of the average magnetization in the nanoalloys, which is in good agreement with the experimental data of Li et al. (*J. Magn. Magn. Mater.* **1997**, *170*, 339). Finally, we show that the value of the orbital-to-spin ratio in both fcc and polyicosahedral Fe−Ni clusters is very sensitive to the internal location of the Fe impurities, a result that suggests that X-ray magnetic circular dichroism experiments can be very useful to reveal precise features of the chemical order in magnetic cluster alloys.

I. Introduction

Bimetallic transition metal (TM) clusters have attracted considerable attention in the last few years because of their novel optical properties,[1] catalytic activity,[2] and magnetic behavior.[3] The interaction between the two components in bimetallic clusters introduces a mutual influence on neighboring atoms and leads to the unique properties reported for these nanoalloys. In fact, from previous experimental and theoretical studies performed on small clusters deposited on metal surfaces,[4] as gas-phaselike species,[5,6] and in solution,[7] it has been clearly established that the properties of cluster alloys are not necessarily given by the average behavior of their corresponding isolated constituents, and that the observed phenomena strongly depends on the precise details of their geometry and composition. Of course, evaluating the role of each one of the previous contributions should be of fundamental importance to fabricate TM-alloyed nanoparticles with a given predetermined chemical configuration, shape, and size, a result that could open unprecedented opportunities for atomic engineering of new nanostructured materials.

As is well known, Fe−Ni alloys are among the most widely used magnetic materials. In particular, the magnetic properties of bulk samples as well as thin films have been extensively analyzed in the literature. Bulk Fe−Ni alloys have revealed to possess many anomalies[8] as a function of the relative composition of Fe and Ni atoms, such as a (i) strongly varying thermal expansion coefficient,[9] (ii) sizable enhancements or reduction in the average magnetic moments,[10] and (iii) large modifications in the lattice constant of the structures.[11] In the case of thin Fe−Ni films, a large amount of experimental studies[12] have underlined also the crucial role played by the surface morphology, thickness, composition, and the temperature of the samples in the determination of relevant quantities such as the orbital moments, exchange coupling, and both the low-energy orientation as well the temperature dependence of the magnetization in the material.

However, despite the above extensive investigations, the magnetic properties and atomic-ordering processes of Fe−Ni alloys in the form of isolated clusters or nanoparticle arrays have not received similar attention. These kinds of nanostructures are also of fundamental importance because of their possible applications as magnetic recording media or to their use as novel catalytic materials. Actually, there are two relatively recent experimental investigations on which we would like to comment and that clearly illustrate also the existence of interesting complex phenomena in these kind of nanoalloys. On the one hand, it has been reported by Li et al.[13] that the saturation magnetization in ultrafine Fe−Ni particles (synthesized by the hydrogen plasma reaction method) is always lower than their

* To whom correspondence should be addressed. E-mail: guirado@ifisica.uaslp.mx.

10.1021/jp7114065 CCC: $40.75
Published on Web 04/08/2008

bulk value for all range of compositions studied. This result is particularly interesting because nanoparticle arrays are characterized by having a reduced local coordination number, a fact that decreases the electronic hoping between neighboring sites, causes a sizable narrowing in the local band widths, and leads to the formation of localized states, which are all factors that favor the existence of large local magnetic moments in the structures. Even if the authors of ref[13] have clearly underlined that surface effects (such as the presence of adsorbed gases and the existence of noncollinear spin configurations in the outermost atomic shells) surely play an important role in the observed behavior, up to now, there is no clear explanation for the considerable weakening of the average magnetization in Fe−Ni nanoparticles obtained in the experimental measurements of Li et al. On the other hand, Parks and co-workers[5] have analyzed the structure of small Fe-dilute Fe−Ni cluster alloys by means of gas adsorption experiments. In this case, the determination of nitrogen saturation levels on the cluster's surface seems to indicate that small Fe−Ni cluster alloys are more stable when the iron atoms are located in the core region of the structures. This is also a very interesting finding because both Fe and Ni atoms have almost the same size and similar surface energies and, as a consequence, upon alloying it is not obvious to expect the existence of surface segregation in favor of a particular species.

At this point, it is important to comment that, even if in bimetallic nanoparticles it is experimentally possible to identify the type and the relative composition of the species involved, even in our days there is no experimental technique capable of accurately determining the local geometrical and chemical structure in these kind of nanoalloys, a fact that seriously limits of course the understanding of the measured data.

Consequently, it is thus of fundamental importance to bring some important details of the atomic structure that go beyond the current experimental evidence and reveal the underlying physics that could be at the origin of the unusual reported magnetic and structural behavior discussed in the previous paragraphs. On the one hand, in Fe−Ni nanoparticles and small clusters, strong finite-size effects are expected and they need to be quantified. On the other hand, it is necessary to explore if there is any strong correlation between chemical order and magnetic behavior in these kind of nanoalloys. Because of the well-known sensitivity of Fe atoms to the local atomic environment (Fe is defined as a nonsaturated magnetic material), under certain conditions the Fe atoms in Fe−Ni cluster alloys[14] may undergo a reduction or an enhancement in its value for the local magnetic moment, they may change the magnitude of the magnetic moment of its neighboring sites, or may lead to the formation of ferromagnetic or antiferromagnetic configurations within the structures, a fact that is expected to strongly perturb the properties of the particles. In particular, it would be interesting to look for those factors that favor the development of reduced magnetization values, or induces the formation of well-defined chemical orderings within the structures, to try to shed some more light into the experimental data of Li et al.[13] and Parks and co-workers.[5] More generally, it will be interesting to analyze if by simply altering the composition ratios as well as the chemical ordering within the particles (e.g., by thermal treatments or low-energy ion scattering experiments), it is possible to obtain various structures with different functionalities.

In the present work, we present thus a detailed theoretical investigation by combining density functional theory (DFT) and tight binding approaches of the magnetic properties of small Fe−Ni cluster alloys having different compositions and chemical orderings. Calculations have been carried out by modeling the Fe−Ni nanoalloys as compact fragments of the fcc lattice as well as small polyicosahedral clusters to determine, by fully relaxing our considered structures, the preferred sites of the Fe atoms and their effect on the magnetic properties. For each one of the Fe-compositions studied, we will consider disordered Fe−Ni-alloyed particles, as well as segregated clusters with a core−shell structure, namely, Fe at the core and Ni in the outer shells and vice-versa. Special attention is paid on the local distribution of the magnetic moments and, with this analysis we have been able to find well-defined spin configurations and chemical orders that can considerably reduce the total magnetization in the system. In addition, we will show that the value of the orbital-to-spin ratio in our Fe−Ni clusters is very sensitive to the internal location of the Fe impurities and conclude that X-ray magnetic circular dichroism measurements[15] can be very useful, besides gas adsorption experiments, to reveal precise features of the chemical order in magnetic cluster alloys. Finally, we will use our theoretical results to try to understand the anomalous magnetic behavior experimentally observed in Fe−Ni nanoparticles by Li et al., as well as to analyze the Fe migration in to the core region on Fe-dilute Fe−Ni polyicosahedral clusters obtained by Parks et al. We believe that the comparison with both experimental results has allowed us to elucidate some electronic and microstructural aspects in the nanoalloys that need to be taken into account to understand the measured data.

The rest of the paper is organized as follows. In Section II, we briefly describe the theoretical models used for the calculations. In Section III, we present the discussion of our results, and finally in Section IV the summary and conclusions are given.

II. Method of Calculation

A. Pseudopotential Approach. The structural and magnetic properties of our considered Fe−Ni cluster alloys have been obtained by means of density functional theory (DFT) calculations using numerical atomic orbitals basis set to solve the single-particle Kohn−Sham equations. For the exchange-correlation potential, we used the Perdew, Burke, and Ernzerhof (PBE) form[16] of the generalized gradient approximation (GGA). The atomic cores were replaced by nonlocal, norm-conserving Troullier−Martins pseudopotentials[17] that were factorized in the Kleinman−Bylander form[18] and included nonlinear core corrections to account for the significant overlap of the core charge with the 3d orbitals as implemented in the SIESTA code.[19] The ionic pseudopotentials were generated using the atomic configurations: $4s^1$, $4p^0$, and $3d^9$ for Ni and $4s^1$, $4p^0$, and $3d^7$ for Fe with corresponding cutoff radius of 2.05(2.00), 2.05(2.00), and 2.05(2.00) au for Ni (Fe). Valence states have been described using double-ζ basis sets with two orbitals having different radial forms to describe both the 3d shells of Ni and Fe as well as one orbital to describe the 4p shell.

We have chosen cluster alloys having a reduced number of atoms (as large as 58 atoms) allowing SIESTA to perform at the same time both the electronic self-consistent calculations and geometrical optimization procedures with a manageable computational requirement. In all calculations, we consider a 22 Å cubic supercell and used a 200 Ry energy cutoff to define the finite real-space grid for numerical integrations. The clusters were allowed to relax without any symmetry (or spin) constraints using a gradient conjugate algorithm until the interatomic forces were smaller that 0.01 eV/Å.

To verify the accuracy of our pseudopotential approximation, we have performed some test calculations on some small pure

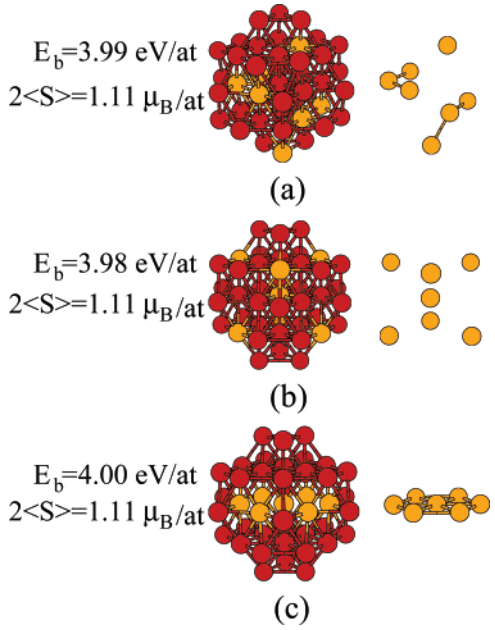

Figure 1. Calculated lowest energy atomic configurations for some representative fcc Fe_7Ni_{36} cluster alloys. We show results for (a) a random distribution of Fe species (yellow spheres), (b) when Fe atoms are segregated on the surface, and (c) for Fe species mainly located in the core region of the structures. To the right of each one of the equilibrium configurations we show only the distribution of the iron atoms [by removing all the Ni species (red spheres) of the structure] to more clearly illustrate the different chemical orders. To the left, we specify the values of the binding energy E_b and average spin moments in each case.

Ni_N and Fe_N clusters, as well as in small Fe−Ni cluster alloys to compare with other DFT calculations available in the literature. For the Ni_2 dimer, we obtain a total spin moment of $2\mu_B$ and a Ni−Ni interatomic distance of 2.14 Å, which nicely compares with the all electron calculations of Castro et al.[20] that gives values of $2\mu_B$ and 2.10 Å, respectively. In addition, they are in very good agreement with the experimental measurements reported in refs 21 and 22 in which values of $2\mu_B$ and 2.16 Å are found for the same quantities. For the Ni_3 cluster, we obtain that an equilateral triangle is the lowest energy atomic configuration with a total spin moment of $2\mu_B$ and Ni−Ni bond length of 2.25 Å, which is in good agreement with the results of ref 20 in which values of $2\mu_B$ and 2.23 Å, respectively, are found. For the Fe_2 dimer, we found values of $6\mu_B$ and 1.95 Å for the total spin moment and interatomic distance respectively, which are very close to the ones obtained in all electron calculations in ref 20 that gives values of $6\mu_B$ and 1.95 Å for the same quantities. These values agree also very nice with the experimental measurements presented in refs 21 and 22 in which values of 6 μ_B for the total spin moment and Fe−Fe bond lengths that vary in the range 1.73−2.04 Å are reported. In the case of Fe_5 (trigonal bipyramid), Fe_7 (decahedral configuration), and Fe_{13} (icosahedral structure), we found average spin values of 3.6, 3.12, and 3.4 μ_B/atom in good agreement with the plane wave calculations performed by Rollmann et al.[23] with the Viena simulation package, which gives values of 3.2, 3.12, and 3.4 μ_B/atom for the same structures. Finally, for the mixed Fe−Ni clusters, we obtain for the Fe−Ni dimer an interatomic distance of 2.08 Å and a total spin magnetization of $4\mu_B$ in good agreement with the data of Rao et al.,[24] which reports exactly the same values. In the case of a $(FeNi)_4$ cluster alloy, we consider the two isomers shown in Figure 2d,e of ref 24. We found an average spin moment of 2 μ_B/atom in both cases in agreement with the results of Rao et al., and a distribution of

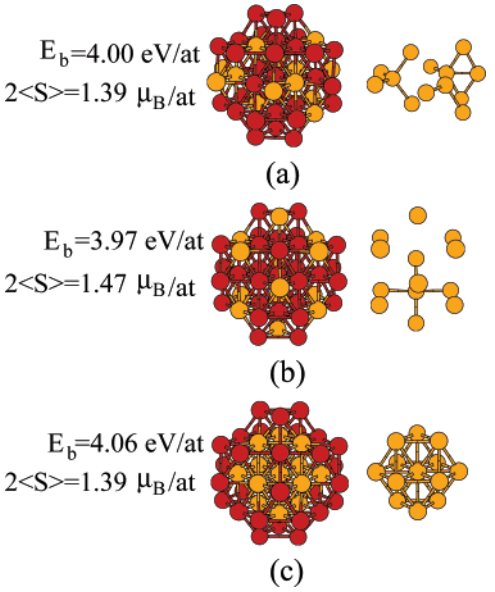

Figure 2. Same as in Figure 1 but for fcc $Fe_{13}Ni_{30}$ cluster alloys.

interatomic distances that vary at most by 6% when compared with the structural data provided in ref 24. Concerning the relative stability between the two considered isomers, we obtain an energy difference of 0.13 eV/atom, very close to the value of 0.14 eV/atom reported in ref 24, being the segregated structure (see Figure 2d of that work) the most stable array. We believe that the previous comparison clearly justifies the use of our pseudopotential approach.

B. Tight Binding Method. Self-consistent semiempirical calculations were carried out to analyze also the local orbital moment distribution as well as to obtain theoretical values for the (easy experimentally accessible) orbital-to-spin ratio in selected Fe-dilute Fe−Ni cluster alloys, by using the realistic d-band tight-binding Hamiltonian, proposed in ref 25 which includes the intra-atomic Coulomb interactions in the unrestricted Hartree−Fock approximation and the effects of the spin−orbit coupling non-perturbatively. The model has been described in detail elsewhere;[26,27] thus, we only summarize its main points and discuss the choice of parameters.

Because of the inclusion of the spin−orbit (SO) interaction, the rotational invariance of the electronic Hamiltonian is no longer preserved and depends now on the orientation δ of the magnetization in the system. In the usual notation, the Hamiltonian is given by

$$H^{\delta} = \sum_{i\lambda,\sigma} \Delta\epsilon_{i\sigma}^{\delta} n_{i\lambda\sigma} + \sum_{i\lambda,j\mu,i\neq j,\sigma} t_{i\lambda,j\mu} c_{i\lambda\sigma}^{+} c_{j\mu\sigma} + \sum_{i,\lambda\sigma,\mu\sigma'} \xi_i(\vec{L}_i \cdot \vec{S}_i)_{\lambda\sigma,\mu\sigma'} c_{i\lambda\sigma}^{+} c_{i\mu\sigma'} \quad (1)$$

where $c_{i\lambda\sigma}^{+}$ ($c_{i\lambda\sigma}$) refers to the creation (annihilation) operator of an electron with spin σ in the d orbital λ at atomic site i and $n_{i\lambda\sigma} = c_{i\lambda\sigma}^{+} c_{i\lambda\sigma}$ defines the electron number operator. The first term of eq 1, $\Delta\epsilon_{i\sigma}^{\delta}$ corresponds to the site- and spin-dependent energy shift of the d level $\epsilon_{i\sigma} = \epsilon_d^0 + \Delta\epsilon_{i\sigma}^{\delta}$ (where ϵ_d^0 stands for the d orbital energy in the paramagnetic bulk) and is determined by the global charge and the spin as follows

$$\Delta\epsilon_{i\sigma}^{\delta} = U(i)\Delta n^{\delta}(i) - \sigma J(i) S_{\delta}(i) \quad (2)$$

with $\Delta n^{\delta}(i) = n^{\delta}(i) - n_d(\text{bulk})$ and $\sigma = +1(-1)$ for spin up(down). The average intra-atomic direct Coulomb repulsion

integral is denoted by U, and the average exchange integral is denoted by J. The spin-quantization axis is taken to be parallel to the magnetization direction, which is assumed to be uniform within the cluster. In the second term of eq 1 $t_{i\lambda,j\mu}$ denotes the corresponding hopping integrals between sites i and j and orbitals λ and μ and finally, the third term corresponds to the spin−orbit (SO) interaction treated in the usual intra-atomic single-site approximation.[28,29] Here, ξ_i stands for the SO coupling constant at atom i (i.e., ξ_{Fe} and ξ_{Ni}) and $(\vec{L}_i \cdot \vec{S}_i)_{\lambda\sigma,\mu\sigma'}$ refer to the intra-atomic matrix elements of $\vec{L}\cdot\vec{S}$ that couple the up and down spin-manifolds and that depend on the relative orientation between the magnetization direction and the cluster lattice. The number of d-electrons at site i

$$n^{\delta}(i) = \sum_{\lambda} (\langle n^{\delta}_{i\lambda\uparrow}\rangle + \langle n^{\delta}_{i\lambda\downarrow}\rangle) \tag{3}$$

and the local spin $\vec{S}(i) = [S_x(i), S_y(i), S_z(i)]$ at each cluster site i and for a given direction of magnetization δ

$$S_{\delta}(i) = \frac{1}{2}\sum_{\lambda} (\langle n^{\delta}_{i\lambda\uparrow}\rangle - \langle n^{\delta}_{i\lambda\downarrow}\rangle) \tag{4}$$

are calculated self-consistently by integrating the local density of states (LDOS) $\rho^{\delta}_{i\lambda\sigma}(\epsilon) = -(1/\pi)\mathrm{Im}\{G^{\delta}_{i\lambda\sigma,i\lambda\sigma}(\epsilon)\}$, where $G^{\delta}(\epsilon) = [\epsilon - H^{\delta}]^{-1}$ is the Green function operator, up to the Fermi level ϵ_F, which is determined by the number of d-electrons per atom in the clusters.

The local orbital moments $L_{\delta}(i)$ at each cluster site are calculated from

$$L_{\delta}(i) = \sum_{\sigma}\sum_{m=-2}^{m=2} \int_{-\infty}^{\epsilon_F} m\, \rho^{\delta}_{im\sigma}(\epsilon) d\epsilon \tag{5}$$

where the real d-orbitals have been transformed to the complex spherical harmonics basis and m refers to the magnetic quantum number. Here, the quantization axis of the orbital momentum is the same as the spin quantization axis.

The LDOS $\rho^{\delta}_{i\lambda\sigma}(\epsilon)$ are determined by performing independent self-consistent calculations for each orientation of the magnetization δ. In all cases, we will consider a magnetization direction, along the z-axis taken as a principal symmetry axis of the particle, as well as one in-plane direction within the xy-plane of the clusters, taken along a nearest neighbor bond. However, it is important to remark that the magnetization direction in the structures can be chosen without restrictions. The LDOS $\rho^{\delta}_{i\lambda\sigma}(\epsilon)$ are computed by using Haydock−Heine−Kelly's recursion method.[30] The number of levels used in the continued fraction expansion of the Green's function is such that the results for $\rho^{\delta}_{i\lambda\sigma}(\epsilon)$ correspond to the exact solution of the single-particle problem.

We can thus conclude this section by saying that we will use an hybrid theoretical methodology to study the magnetic properties of our considered Fe−Ni cluster alloys in which the energetics, structural properties, and spin moment contributions are obtained by means of a DFT approach, while the more complex calculations involving the determination of the orbital moments in our Fe−Ni nanoalloys will be performed by means of a realistic tight binding model.

III. Results and Discussion

A. Relative Stability and Structural Properties of fcc Fe−Ni Cluster Alloys. In Figures 1, 2, and 3, we show first the equilibrium structures found within the SIESTA methodology

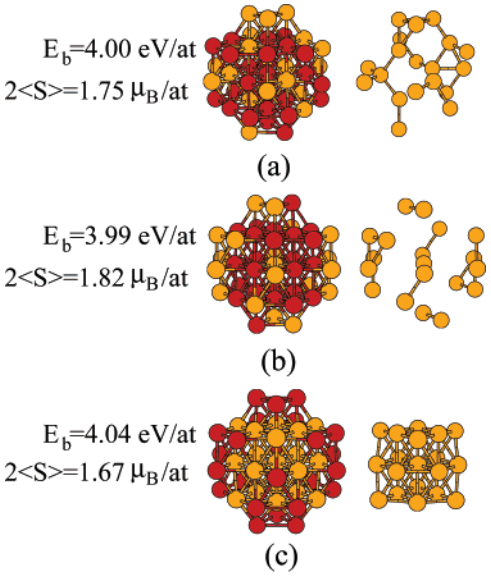

Figure 3. Same as in Figure 1 but for fcc $Fe_{19}Ni_{24}$ cluster alloys.

for some representative fcc Fe−Ni nanoalloys, namely: fcc Fe_7Ni_{36}, $Fe_{13}Ni_{30}$, and $Fe_{19}Ni_{24}$ clusters with different chemical orders. In the figures, we have considered a 43-atom fcc Ni particle, built by adding to a central atom its successive first, second, and third nearest neighbor shells j, in which we have included 7, 13, and 19 Fe atoms in random configurations (Figures 1a, 2a, and 3a), by assuming atomic arrays in which a complete surface segregation of the Fe atoms is present in the particles (Figures 1b, 2b, and 3b) and finally, by considering core−shell configurations where Fe species are confined to the center of the structures surrounded by Ni atoms (Figures 1c, 2c, and 3c). We would like to comment that we always consider three different atomic arrays for each one of the compositions and chemical orders studied, and that the structures shown in Figures 1−3 correspond to the most stable atomic configurations. However, for 13 and 19 Fe atoms forming a core(Fe)−shell(Ni) array, only one atomic configuration was analyzed because in those cases it is possible to construct perfect closed-shell structures (see Figures 2c and 3c].

As stated in Section II, all our considered cluster alloys have been fully optimized without symmetry or spin constraints until the interatomic forces were smaller than 0.01 eV/Å. In addition and for the sake of clarity, we plot to the right of each one of the equilibrium configurations only the distribution of the iron species within the 43-atom structure (by removing the Ni atoms of the particle) with the purpose of more clearly illustrating each one of the different chemical orders. Finally, in the left side we specify also the values of the binding energy E_b and average spin moment per atom $2\langle S\rangle$ obtained for each cluster alloy.

Interestingly, for these three Fe compositions (as well as for the rest of our considered alloys), the lowest energy atomic configurations are always found when the Fe species are located in the core region of the particles (see Figures 1c, 2c, and 3c) forming a compact structure (see the right column in all cases), being more stable than the other chemical arrays by values as large as 2.4 eV. The here-obtained phase separation is very interesting because both Fe and Ni atoms have almost the same size and similar surface energies and it is thus not easy to establish a priory the existence of a surface segregation in favor of a particular species. However, this result is in line with the experimental studies of Parks et al.[5] performed on small Fe-dilute Fe−Ni clusters that have concluded, by means of gas adsorption experiments, that the Fe impurities are located in

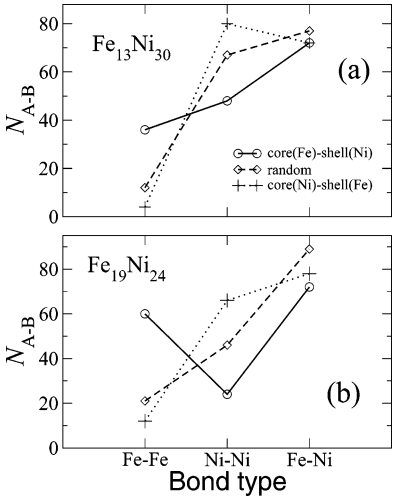

Figure 4. Number of Fe−Fe, Ni−Ni, and Fe−Ni bonds for the lowest energy (a) $Fe_{13}Ni_{30}$ and (b) $Fe_{19}Ni_{24}$ cluster alloys shown in Figures 2 and 3, respectively.

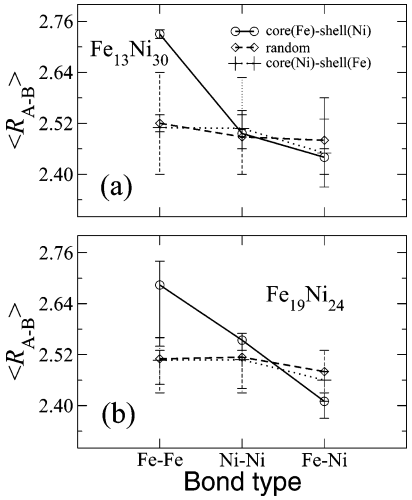

Figure 5. Average bond lengths for Fe−Fe, Ni−Ni, and Fe−Ni pairs for the lowest energy (a) $Fe_{13}Ni_{30}$ and (b) $Fe_{19}Ni_{24}$ cluster alloys shown in Figures 2 and 3, respectively.

the inside of the particles, a result that has been recently theoretically corroborated by Longo et al.[31] through DFT calculations. Actually, it is important to mention that both experimental and theoretical studies reported in refs 5 and 31, respectively, conclude that the structure of these Fe-dilute Fe−Ni cluster alloys, at least up to 26 atoms, is polyicosahedral in nature and in this sense, our results shown in Figures 1, 2, and 3 for fcc particles seems to reveal a more general trend because Fe migration into the core region of the clusters appears thus to be independent of the particle's geometry. Interestingly, from our calculations we have found that, when increasing the concentration of Fe atoms in the system (up to 63%), the clustering of iron species in the center of the particles is still preferred, leading to the formation of a perfect core(Fe)−shell(Ni) structure. In fact, in the particular case of the $Fe_{13}Ni_{30}$ cluster alloy, for which it is possible to construct a perfect core(Fe)−shell(Ni) configuration (see Figure 2c), we have allowed up to 3 Fe atoms, belonging to the first shell of neighbors surrounding the central Fe site, to exchange places with nearest neighbors Ni atoms of the overlayer (not shown). With this procedure, we destroy the perfect core(Fe)−shell(Ni) structure (see Figure 2c) and allow some intermixing between the pure Fe and Ni regions. From our total energy calculations, we found that the total energy of these systems increases by values as a large as 1.7 eV, clearly implying the complete inmiscibility of the two components when alloyed as small particles.

It is important to remark that the here-obtained relative stability between the different chemical configurations is strongly correlated with the different concentrations of Fe−Fe, Fe−Ni, and Ni−Ni bonds in the clusters. This is seen from Figure 4 where we plot, for each one of the considered chemical orders in the $Fe_{13}Ni_{30}$ (Figure 2) and $Fe_{19}Ni_{24}$ (Figure 3) alloys, the amount of Fe−Fe, Fe−Ni, and Ni−Ni pairs, N_{Fe-Fe}, N_{Fe-Ni}, and N_{Ni-Ni} respectively. From Figure 4a,b, we notice that the lowest energy atomic configurations, denoted by a continuous line, are characterized by having the largest number of Fe−Fe bonds (as seen also from Figures 2c and 3c) and the lowest number of Ni−Ni pairs. Actually, the energy gain obtained when we move an Fe_2 dimer placed as a substitutional impurity on the surface of a Ni_{43} cluster to the core region of the structure is of the order of ∼0.4 eV. This energy value together with the results shown in Figure 4 clearly point also to the clustering of iron atoms, the low miscibility of both Fe and Ni species, and the Fe migration into the core region of the structures.

Actually, the next favorable atomic configurations correspond to chemical orders as the ones shown in Figures 1a, 2a, and 3a where at least some degree of Fe aggregation (even if does not occurs in the core region) is present within the structures. In fact, the previous qualitative arguments are similar to the ones typically used in theories such as the second moment approximation[32,33] in which the different concentration of Fe−Fe, Ni−Ni, and Fe−Ni pairs plays a fundamental role in the energetics of the alloys. Furthermore, and in analogy with bulk systems, the calculation of the order parameter η defined as[34]

$$\eta = \frac{N_{Fe-Fe} + N_{Ni-Ni} - N_{Fe-Ni}}{\text{total of pairs}} \tag{6}$$

for the lowest energy chemical orders specified in Figure 4a,b yields η values >0 and equal to ∼0.07, which are values that imply also the formation of a segregated alloy in agreement with our total energy calculations.

Finally, it is important to mention that the different chemical orders in our 43-atom fcc cluster alloys shown in Figures 1−3 have a strong influence on the structural parameters of the particles. In Figure 5, we show our results for the average interatomic bond length (together with their corresponding error bars) between Fe−Fe ($\langle R_{Fe-Fe}\rangle$), Ni−Ni ($\langle R_{Ni-Ni}\rangle$), and Fe−Ni ($\langle R_{Fe-Ni}\rangle$) pairs obtained from the $Fe_{13}Ni_{30}$ and $Fe_{19}Ni_{24}$ alloys. From the figures, we can see that although for disordered and core(Ni)−shell(Fe) arrays the values for $\langle R_{Fe-Fe}\rangle$, $\langle R_{Ni-Ni}\rangle$, and $\langle R_{Fe-Ni}\rangle$ are almost the same, being of the order of the arithmetic weighted mean of bulk Fe−Fe and Ni−Ni pairs, in the lowest energy core(Fe)−shell(Ni) configurations the value for $\langle R_{Fe-Fe}\rangle$ is found to be considerably large, being expanded by 7−9% with respect to the corresponding bulk fcc value. These strong variations in the nearest neighbor interatomic distances in the particles shown in the figure leads of course to the existence of a highly nonuniform relaxation profile within the structures that surely will play a fundamental role in determining the electronic behavior and catalytic properties of the cluster alloys. In particular, the sizable expansion that occurs in the core region is expected to increase the electron localization in the system a fact that, as will be seen in the following, will lead to the formation of a local moment distribution with high magnetization states. Interestingly, it is important to comment that in our lowest energy atomic configurations (see Figures 1c, 2c, and 3c), the notable increase in the $\langle R_{Fe-Fe}\rangle$ values is directly

correlated with the presence of the Ni overlayer, because in the case of uncovered fcc Fe_{13} and Fe_{19} clusters, $\langle R_{Fe-Fe} \rangle$ is of the order 2.54 Å, which is very close to the iron fcc bulk value.

B. Magnetic Properties of fcc Fe−Ni Cluster Alloys. In this section, we present our DFT calculations dedicated to analyze the magnetic properties of our considered Fe−Ni cluster alloys. In the previous section, we have already found that the total energy as well as the structural properties of fcc Fe−Ni clusters are highly dependent on the precise details of the chemical ordering, defining the existence of highly stable atomic configurations (i.e., Fe−Ni alloy clusters achieve their best stability when iron atoms are located in the core region of the particles forming a compact structure) together with well-defined structural changes induced by alloying. However, in contrast to the strong sensitivity of the energetics and structural parameters we have obtained from our spin-polarized electronic structure calculations that in the Fe-dilute regime the total spin magnetization $2\langle S \rangle$ in the cluster alloys is insensitive to sizable changes in the chemical order within the particles. For example, for the Fe composition shown in Figure 1 (16% of Fe), we have found values for $2\langle S \rangle$ equal to $48\mu_B$ in all our (contrasting) considered Fe_7Ni_{36} cluster alloys (see Figure 1a−c) for representative examples). Similarly, for Fe_9Ni_{34} (21% of Fe) particles (not shown) a constant value of $52\mu_B$ has been found. These results are very interesting because in bimetallic transition metal clusters the value of $2\langle S \rangle$ is expected to be significantly affected by the precise details of the local atomic environment, as is well known.

At this point, it is important to comment that the previous magnetic behavior is in agreement with recent theoretical calculations reported by Rao et al.[24] performed on very small Fe_nNi_m ($n + m = 8$) clusters in which they have also found that the total spin magnetization is independent of the atomic configuration of Fe and Ni atoms within the clusters. This fact has been attributed to the large energy gap between the minority and majority highest occupied molecular orbitals, an energy difference that prevents, when the structure or the local chemical order is varied, the existence of energy level inversions in the electronic spectra that could modify the spin-dependent electronic occupations, maintaining as a consequence the same value for $2\langle S \rangle$ in all the cluster alloys.

Complementary to these arguments we would like to add that, due to the similar electronegativities of both Fe and Ni species, a very small charge transfer is expected, and in fact we have found local variations in the electronic occupations as large as 0.1 *e* defining thus our Fe-dilute Fe−Ni cluster alloys as weakly interacting systems. Actually, we have obtained that the local spin moments of Fe(Ni) atoms are almost insensitive to the number of surrounding Ni(Fe) species. This is clearly seen from Figure 6 where we show for random Fe_7Ni_{36} (Figure 6a) and Fe_9Ni_{34} (Figure 6b) cluster alloys the values of $2S_x(i)$ (x = Fe and Ni) at some selective sites, being characterized by contrasting local chemical environments. From Figure 6a, we see that the two Ni surface sites $i = 1$ and 2 (marked with arrows), which differ in the number of surrounding Fe atoms, namely, 3 and 0 Fe's, respectively, present small variations in the local spin values of the order of $0.03\mu_B$. This is also the case for the surface sites labeled as $i = 3$ and 4 in the same figure, which correspond now to Fe species, where the two $2S_{Fe}(i)$ values vary by $0.11\mu_B$. Similarly, in the Fe_9Ni_{34} cluster alloy (Figure 6b) the same range of variations for the local moments of Ni(Fe) atoms placed in contrasting chemical environments are found, and consequently we can define thus the total spin magnetization

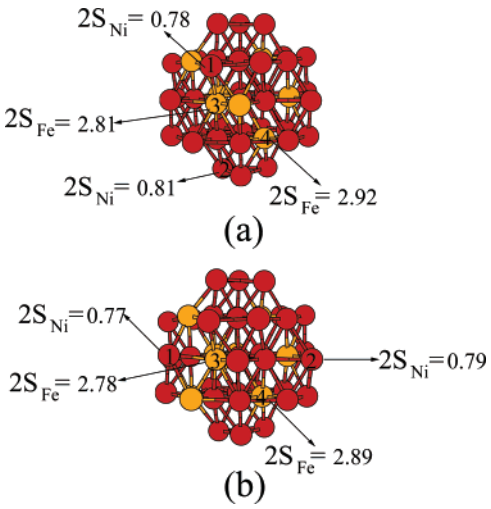

Figure 6. Calculated values for the local spin moments, $2S(i)$, at some selective sites i (see text) for the lowest energy (a) Fe_7Ni_{36} and (b) Fe_9Ni_{34} cluster alloys shown in Figures 1a and 2a, respectively.

of our Fe-dilute Fe−Ni alloys as being the result of almost independent local contributions.

However, it is important to demonstrate that even if the total number of electrons, for example, in sites $i = 3$ and $i = 4$ shown in Figure 6a, is almost the same (8.07 *e* for $i = 3$ and 8.05 *e* for $i = 4$) we have found that there are more notable variations in the intrasite spin-polarized electronic occupations of the s-, p-, and d-bands of each atom. For example, for the Fe species located at site $i = 3$ the electronic configuration for the spin-up orbitals is $d_\uparrow^{4.789} s_\uparrow^{0.302} p_\uparrow^{0.352}$, and for the spin-down orbitals the electron configuraton is $d_\downarrow^{1.958} s_\downarrow^{0.308} p_\downarrow^{0.369}$, which yields a total number of electrons equal to 8.07 and a local spin moment of $2.81\mu_B$. However, for $i = 4$ we have $d_\uparrow^{4.817} s_\uparrow^{0.307} p_\uparrow^{0.366}$ and $d_\downarrow^{1.895} s_\downarrow^{0.303} p_\downarrow^{0.368}$, an electronic configuration that even if it yields a value of 8.05 for the total number of electrons, it gives a value for $2S_{Fe}(i = 4)$ of $2.92\mu_B$. Clearly, these kind of variations in the spin-polarized intrasite electronic occupations are at the origin of the small changes observed in the local spin moments at the different Fe locations in the structures. Finally, it is important to comment also that even if the local spin moment distribution is not very sensitive to the local chemical order, it follows the well-known dependence with the local coordination number, being both $2S_{Ni}(i)$ and $2S_{Fe}(i)$ moments more enhanced-(reduced) at the less(more) coordinated sites in the structures.

Interestingly, with increasing the concentration of Fe species in the particles, the previous constant behavior for $2\langle S \rangle$ for different atomic configurations is no longer observed, and variations in the total spin magnetization start to appear among the different cluster alloys. This is clearly seen from Figure 7 where we plot, as a representative example, the total spin moment $2\langle S \rangle$ (Figure 7a) as well as the binding energy E_b (Figure 7b) as a function of the chemical order for various Fe_{19}-Ni_{24} isomers. Furthermore, as insets we include in Figure 7a only the distribution of Fe atoms within the 43-atom particles to illustrate the different considered chemical orders. From Figure 7(a), we notice variations in $2\langle S \rangle$ as large as $6\mu_B$, the largest reductions being found in configurations I and III, which are characterized (see the corresponding insets) by having the largest degree of clustering of Fe species. We can understand this behavior by recalling that Fe is known as a nonsaturated magnetic material, and as a consequence a notable accumulation of these species in a well-defined region of space could produce sizable reductions in $2\langle S \rangle$. This kind of magnetic behavior has been previously found in clusters,[35] as well as in thin films and

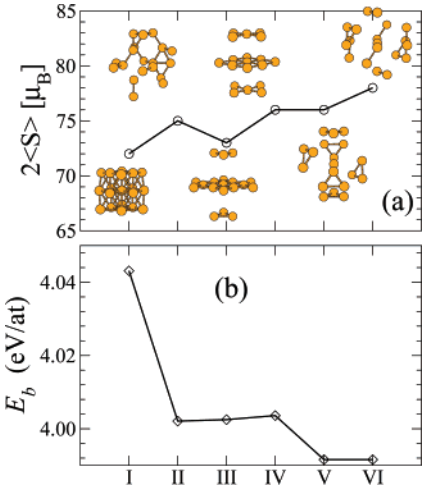

Figure 7. (a) Calculated total spin magnetization and (b) binding energies E_b for different $Fe_{19}Ni_{24}$ cluster alloys (I−VI). In (a) we show as insets only the distribution of the Fe species within the 43-atom structure to more clearly illustrate the different chemical orders.

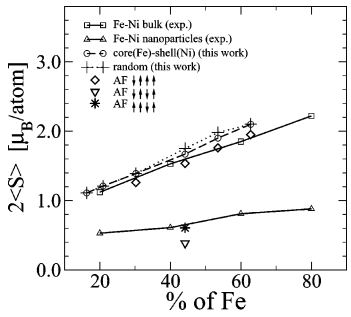

Figure 8. Calculated average spin moment per atom of 43-atom Fe−Ni cluster alloys as a function of the Fe content and for different chemical configurations: random and core(Fe)−shell(Ni) atomic arrays (see Figures 1−3 for representative examples). We also include, as isolated points, values for the average spin moment in some of our cluster alloys with various types of antiferromagnetic configurations.

multilayered structures,[12] and clearly illustrate the strong dependence of the magnetic properties on the local atomic environment of these Fe-based nanostructures. Notice that the highest enhancements in $2\langle S\rangle$ is obtained in configuration VI in which we have a distribution of Fe atoms that are in general isolated on the surface of the clusters, a fact that increases the electron localization in the structures and leads to a sizable enhancement of the local spin moments. We can thus conclude by saying that as a general trend for a given concentration of Fe species in a Fe−Ni nanoparticle alloy, iron clustering within the structures tends to lower the average magnetization when compared to that of random configurations or ordered alloys (see Figure 7a).

Finally, notice from Figure 7b that the binding energy as a function of the chemical order follows the trends already found in Figures 1−3 in which aggregation of Fe species within the particles increases the values of E_b, mainly when this clustering occurs in the core region of the structures (see results for configuration I in Figure 7b).

To summarize our results, we show in Figure 8 our theoretical data for the average spin magnetization $2\langle S\rangle$ as function of the Fe composition in all our considered fcc 43-atom fcc Fe−Ni cluster alloys. In the figure, we also include for the sake of comparison some representative points of the measured average magnetization data for Fe−Ni bulk alloys as well as for fcc Fe−Ni nanoparticle samples reported by Li et al.[13] (see Figure 8 of their work). The most important feature to remark from the figure is that as expected the average spin moments $2\langle S\rangle$ of all our considered isolated Fe−Ni cluster alloys are enhanced with respect to the bulk value for the same composition. This is clearly in contrast with the experimental data obtained for Fe−Ni nanoparticles shown also in the figure for which a notable reduction in $2\langle S\rangle$ has been found. At this point, it is important to comment that the mechanism responsible for the considerable weakening of the average magnetization in the Fe−Ni nanoparticles synthesized by Li et al. is still not clear, and it is thus interesting to look, within our theoretical framework and model systems, for the underlying physics that could favor the development of such reduced values for $2\langle S\rangle$.

First, it is important to comment that, even if in the Fe−Ni nanoparticles synthesized in ref 13 it has been possible to estimate the size, crystallographic structure, and chemical composition of the samples, it has been always very difficult to experimentally obtain information related to the precise details of the local atomic environment such as for example the distribution of both Fe and Ni species within the particles. From our calculations discussed in the previous paragraphs, we have found that for a well-defined concentration of Fe atoms, different chemical orderings can have an important effect on the total spin magnetization of the cluster alloys. In particular, we have obtained that the clustering of the iron atoms in well-defined regions of the structures is preferred and leads to the formation of local moments with reduced spin values affecting the global magnetic properties of the cluster alloys (see Figure 7a). However, these well-defined volumes with reduced magnetizations are not enough, at least in our fcc 43-atom cluster alloys, to produce dramatic reductions in $2\langle S\rangle$ when compared with the bulk magnetization data (see Figure 8).

Interestingly, in this respect it is important to comment that there is a well-known tendency of iron materials adopting an fcc structure to prefer the antiferromagnetic (AF) order.[36] In this case, the antiparallel alignment of the spin moments within the material naturally leads to an additional lowering of the average magnetization and, if present in some of our considered cluster alloys, it could be also (besides the clustering of the Fe species within the particles) an important source of reduction in the $2\langle S\rangle$ values. Consequently, we have decided to analyze the stability of some possible AF solutions in our highly stable core(Fe)−shell(Ni) $Fe_{13}Ni_{30}$, $Fe_{19}Ni_{24}$, $Fe_{23}Ni_{20}$, and $Fe_{27}Ni_{16}$ cluster alloys by simply turning down the orientation of the spin moment of the central Fe atom to yield spin configurations of the type ↓↑↑↑. However, only for the $Fe_{19}Ni_{24}$ structure we will study additional AF configurations such as: ↑↑↓↑ and ↓↑↓↑ in which antiparallel alignment between atoms in different atomic shells is considered. From these calculations, the most important features to note are that (i) AF spin configurations in our cluster alloys are not energetically preferred (being less stable by values as large as 1.7 eV) and, as expected, (ii) they lead to considerable quenchings in the $2\langle S\rangle$ value as shown in Figure 8. Interestingly, the analysis of the local moment distribution in these AF arrays reveals that the magnitude of the spin moments at the Fe sites $|2S_{Fe}(i)|$ varies in the range of 2.77−3.4 μ_B, although in contrast the local contributions at the Ni atoms are considerably reduced, being in the range of 0.29−0.38μ_B. The previous sizable quenching of the local spin moments at the Ni sites induced by the AF order at the pure Fe regions is very interesting and represents a new and major contribution for the pronounced reduction found for $2\langle S\rangle$ in Figure 8.

At this point, it is important to comment that it was not the purpose of our study to perform an extensive search of all the possible AF solutions present in our considered Fe−Ni particles.

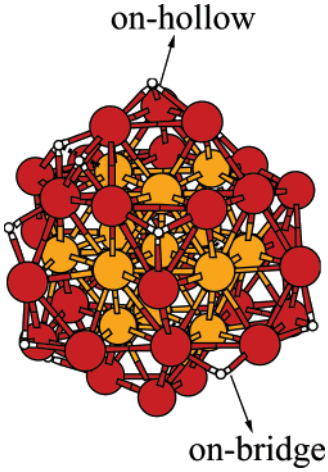

Figure 9. Calculated lowest energy atomic configuration for the core-(Fe)−shell(Ni) $Fe_{13}Ni_{30}$ cluster alloy with 15 hydrogen atoms (white spheres) randomly chemisorbed on its surface.

When exploring AF spin configurations in magnetic clusters, the determination of the lowest energy AF array is a delicate task, especially in systems with a large number of atoms and low symmetry as the ones considered in our work. Consequently and as stated above, in Figure 8 we only plot the average magnetic moment of some possible AF arrays to simply show their effect on the global magnetic behavior. However, even if the here-obtained AF solutions are not energetically preferred, it is well known that the energy difference between ferromagnetic and AF (or more complex) spin arrays can be modified by structural transformations, size effects, or by the adsorption of various gases.[37] The previous facts (which are not explored in our work) could occur in real samples and might lead to the existence of stable AF solutions inducing, as shown in Figure 8, a sizable drop in the average magnetization in Fe−Ni nanoalloys.

Actually, it is important to remark that in the measured magnetization data on Fe−Ni nanoparticles versus the Fe content reported by Li et al.,[13] even in the case of pure Ni and Fe particles, reduced values in the average magnetic moment per atom are found. By looking at Figure 8 of ref 13, we see that pure Ni(Fe) nanoparticles have average magnetizations that are reduced by ∼38%(22%) with respect to the measured bulk nickel(iron) value. The authors argue that because of the experimental procedure used for the synthesis of the Fe−Ni nanoalloys (hydrogen plasma reaction method), the presence of adsorbed gases on the surface of the particles is highly probable and could be also responsible for the low magnetization values observed as a function of the Fe content. Consequently, we have decided to study also the role played by hydrogen surface chemisorption on the magnetic properties of our Fe−Ni cluster alloys as well as to analyze their properties of our nanoalloys in more operating environments. In this case, we will perform additional calculations by considering, as a particular example, the highly stable core(Fe)−shell(Ni) $F_{13}N_{30}$ particle shown in Figure 2c with 15 hydrogen atoms randomly chemisorbed on its surface. In Figure 9, we show the fully optimized atomic configuration for the core(Fe)−shell(Ni) $Fe_{13}Ni_{30}H_{15}$ compound. From the figure, we notice that the inclusion of the H atoms leads to the formation of a highly distorted structure, when compared to the uncovered one shown in Figure 2c, where most of the atoms of the cluster structure perform lateral displacements as well as upward and inward relaxations to minimize the total energy of the system. It is important to remark that hydrogen atoms are found to be chemisorbed in two configurations (marked with arrows) on the particle's surface, namely, on-bridge, over a Ni−Ni bond, and on-hollow, in the center of a triangular array of Ni atoms, with Ni−H bond lengths that vary in the range of 1.62−1.85 Å, and which are of the order of the ones found in previous works addressing the H chemisorption on pure Ni surfaces[38] and nanoparticles.[39]

With respect to the magnetic properties, we would like to comment that the presence of chemisorbed hydrogen atoms reduces as expected the total spin magnetization from $60\mu_B$, obtained for the hydrogen-free atomic configuration shown Figure 2c, to $56\mu_B$ for the compound shown in Figure 9, implying a 7% of reduction in $2\langle S\rangle$. In fact, the H atoms are found to be weakly polarized with local $2\ S_H(i)$ values as large as $0.07\mu_B$, while the spin moments at the Ni atoms just below the hydrogen species are considerably quenched with values that are in the range of $0.52-0.44\mu_B$, being thus at the origin of the here-obtained sizable reduction in $2\langle S\rangle$. As expected, we can thus conclude by saying that the presence of adsorbed gases on the surface of Fe−Ni nanoalloys could be also a notable factor of reduction in the average magnetization in these kind of systems. Actually, the number of chemisorbed hydrogens considered in Figure 9 define a relatively low covered surface, and consequently it is expected that in Fe−Ni nanoparticles with H-saturated external atomic shells that the quenching of the average magnetization should be more pronounced.

Finally, it is important to comment about the role of temperature on the magnetization meassurements performed on Fe−Ni nanoparticles by Li and co-workers.[13] In Figures 5 and 6 of ref 13, the authors present the saturation magnetization of the synthesized Fe−Ni nanoparticles obtained at 4.5 K and at room temperature, respectively. From both figures, it is clearly observed that in general the magnetization meassurements performed at 4.5 K are almost unchanged with increasing the temperature T up to 300 K. Actually, only in the case of the Fe−Ni nanoalloy containing 60% of Fe, it is observed a continuous decrease in the saturation magnetization, inducing a reduction of about 20% at 300 K. These results are very important because on the on hand they show that varying the temperature of the samples does not play an important role in determining the average magnetization behavior, and that on the other hand the low-temperature results can be thus extrapolated in general to ambient conditions.

We would like to conclude the discussion of this section by saying that, even if not strictly comparable, the present small-cluster results could be useful to analyze the interesting experimental study of the magnetic properties of Fe−Ni nanoparticles reported by Li et al.[13] Within our theoretical framework and model systems, we speculate that the anomalous magnetic behavior obtained in ref 13 for Fe−Ni nanoalloys could be attributed to a complex interplay between the possible existence of (i) iron clustering in the as synthesized Fe−Ni nanoalloys, (ii) the possible formation of antiferromagnetic configurations within the Fe-rich volumes of the particles, and (iii) the presence of adsorbed gases on the surface of the structures. Of course, the simultaneous contributions of the previous effects would lead to an even larger decrease in the total magnetization of the Fe−Ni nanoparticle alloys and could be thus used to understand the unusual magnetic behavior observed in ref 13.

C. Tight-Binding Determination of the Orbital-to-Spin Ratio in Fe-Dilute fcc Fe−Ni Alloys. Finally, it is important to comment that even if our density functional theory calculations indicate that in fcc Fe−Ni cluster alloys the formation of core(Fe)−shell(Ni) arrays are energetically preferred, it is clear

from the experimental point of view that for different synthesis conditions contrasting chemical orders can be obtained within the particles. In this respect, even if gas adsorption experiments[5] have demonstrated to be a useful tool for analyzing well-defined details of the chemical order in different types of bimetallic nanoalloys, it is also clear that they are not able to reveal more precise information concerning the local chemical order within the particles thatcan have a dramatic effect on the measured average magnetization data, as we have shown in this work.

At this point, we would like to comment that recently X-ray magnetic circular dichroism (XMCD) experiments have revealed to be a powerful technique to obtain an acceptable characterization in composite materials.[15] In this technique, the application of the sum rules in the analysis of the XMCD measurements relates the measured spectra to the value of the spin 2*S* and orbital *L* magnetic moments per atom and actually, the study of their ratio, *L*/2*S*, as a function of composition and structural parameters of the samples gives valuable information concerning precise microstructural features. In fact, because of the element sensitivity of XMCD, the properties of well-defined chemical species can be explored. This has been clearly established for example in the case of Fe−Pd thin films[40] where strong variations have been found for the orbital-to-spin ratio at the Fe sites due to sizable changes in the chemical order within the material.

Here, we have thus decided to theoretically analyze the orbital-to-spin ratio in our considered fcc Fe−Ni cluster alloys by calculating the orbital contributions *L* to the total magnetization with the use of the tight binding Hamiltonian *H* presented in Section II B in which it has explicitly included the spin−orbit (SO) interaction term (see eq 1) in a nonperturbative fashion. The inclusion of the SO contribution breaks the rotational invariance of the electronic Hamiltonian and *H* depends now on the orientation of the magnetization δ in the system with respect to the cluster lattice. Finally, as stated in Section II, the component of the local orbital moment $L_\delta(i)$ on the direction δ at each cluster site *i* is obtained from eq 5, while the local spin moments $2S_\delta(i)$ are found by subtracting the spin- and direction-dependent electronic occupation as defined in eq 4.

Briefly, the parameters used for the calculations on Fe−Ni cluster alloys are the following. The two-center d-electron hopping integrals between atoms of the same element (i.e., Ni−Ni and Fe−Fe) are given by the canonical expression[41] in terms of the corresponding bulk d-band widths of the elements involved in the cluster alloys,[42] namely, $W_b(\mathrm{Fe}) = 6.0$ eV and $W_b(\mathrm{Ni}) = 5.0$ eV. On the other hand, the heteronuclear hoppings integrals (Fe−Ni) are obtained as the geometric average of the corresponding homonuclear hopping integrals. This has been proved to be a very good approximation in calculations for embedded clusters,[43] bulk alloys[44] and multilayers[45] of transition metals. The intra-atomic exchange integral *J* is chosen to yield the proper magnetic moment and exchange splittings in the bulk at $T = 0$ [$J(\mathrm{Fe}) = 0.67$ eV and $J(\mathrm{Ni}) = 0.5$ eV] with bulk d-band fillings of $n_d(\mathrm{Fe}) = 7.0$ and $n_d(\mathrm{Ni}) = 9.0$ as used in previous works.[46] Charge-transfer effects are treated in the limit of large direct Coulomb repulsion *U* [i.e., $U(i) \rightarrow +\infty$ and $\Delta n^\delta(i) \rightarrow 0$ with $U(i)\Delta n^\delta(i)$ finite], which amounts to impose local charge neutrality at each site *i*. This approximation is well justified in this case due to the similar electronegativity of both elements which, as already stated in Section III B, is at the origin of the negligible charge-transfer obtained in our all here-considered Fe−Ni cluster alloys. Finally, the corresponding values of the SO coupling constants are taken from ref 29 ($\xi_{\mathrm{Fe}} = 0.05$ eV and $\xi_{\mathrm{Ni}} = 0.11$ eV).

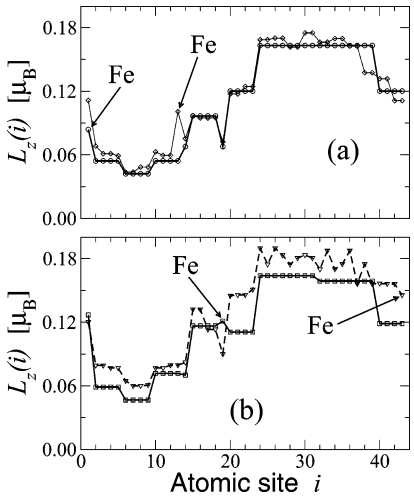

Figure 10. Calculated local orbital moments $L_z(i)$ as a function of atom *i* for the single Fe-doped $FeNi_{42}$ cluster alloy. In (a) we show results for the Fe atom (marked with an arrow) located in the center ($j = 1$) and in the first shell of neighbors ($j = 2$) of the structure whereas in (b) the iron impurity is positioned in the second ($j = 3$) and third shell of neighbors ($j = 4$) of the particle.

As a representative example, we have decided to analyze the local orbital moment contributions $L_\delta(i)$ for the case of a single Fe species included as a substitutional impurity in a fcc 43-atom Ni cluster. In the calculations, we will consider the single Fe atom (i) located in the center of the structure as well as (ii) in each one of the nearest neighbor shells *j* of the particle to look for the existence of well-defined features in the values of L_δ^{Fe} and in the ratio $L_\delta^{\mathrm{Fe}}/2S_\delta^{\mathrm{Fe}}$ characterizing the different internal positions of the iron impurity. In all calculations, we choose the direction $\delta = z$, which is along a principal symmetry axis of the particle. First, it is important to comment that in agreement with our magnetization data discussed in Section III B our tight binding calculations reveal that the average spin moment in our single Fe-doped Fe−Ni alloys is almost independent of the internal location of the Fe impurity having values that vary in the range of 0.9−1.0 μ_B/atom in all our considered chemical orders. This value for the average magnetization per atom is very close to the one found within the SIESTA methodology that yields a $2\langle S\rangle = 0.9$ μ_B/atom for a single Fe atom placed in both the center and surface of the same cluster alloy. In both types of calculations, the value for the local moment of the iron impurity located in the center of the cluster is equal to $3\mu_B$, In contrast, when the Fe atom is at the surface of the particle, the tight binding calculation still yields a value of $3\mu_B$, while the DFT data gives a local spin moment of $3.35\mu_B$. In this case, it is important to comment that the more enhanced value obtained for $2S_{\mathrm{Fe}}(i)$ in the DFT calculation is due to a sizable (additive) contribution of the sp electrons ($0.15\mu_B$), which are absent in our considered semiempirical model. However, notice that the d orbital contributions are almost the same in both theoretical approaches.

Concerning the distribution of the local orbital moments within our single Fe-doped 43-atom Fe−Ni cluster alloys, we show in Figure 10 the calculated values for both $L_z^{\mathrm{Fe}}(i)$ and $L_z^{\mathrm{Ni}}(i)$ in all the sites of the particles and where the values of the orbital moment at the Fe atoms are marked with arrows for clarity. From the figure, we notice that in contrast to the constant dependence of the local spin moments at the Fe sites, the orbital contributions are very sensitive to the local atomic environment,

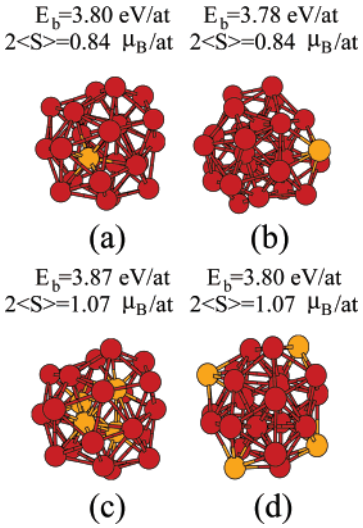

Figure 11. Calculated lowest energy atomic configurations for $FeNi_{25}$ and Fe_4Ni_{22} polyicosahedral clusters. In (a) and (c) the iron impurities are occupying the core region of the structures, whereas in (b) and (d) an iron surface segregation is assumed. The values of the binding energy E_b and average spin magnetization are also specified in each case.

changing from 0.08→0.10→0.12→0.14μ_B as the Fe impurity moves from the atomic shell $j = 1 \rightarrow 2 \rightarrow 3 \rightarrow 4$ as well as inducing strong perturbations at the $L_z^{Ni}(i)$ values of the surrounding Ni atoms. Interestingly, notice that the magnitude of $L_z^{Fe}(i)$ at the central site and at the first shell of neighbors (see Figure 10a) are already of the order of the one obtained at the Fe bulk, where XMCD measurements give an orbital moment of 0.09μ_B,[47] clearly implying the local character of this quantity.

By using the results of Figure 10, it is now possible to calculate the (easily) experimentally accessible orbital-to-spin ratio for the iron species $L_\delta^{Fe}/2S_\delta^{Fe}$ at the four chemical configurations investigated for single Fe-doped fcc Fe−Ni cluster alloys. In fact, from our theoretical data we have found clear differences in this quantity when the Fe atoms are in the core region or at the surface of the particles. Actually, we obtain that the values for $L_\delta^{Fe}/2S_\delta^{Fe}$ vary from 0.028→ 0.035→0.042→0.047 when the location of the iron impurity changes from the atomic shells $j = 1 \rightarrow 2 \rightarrow 3 \rightarrow 4$. This observed behavior is clearly due to the strong variations of the orbital magnetic moment because the spin values stay always constant and equal to 3.0μ_B. Consequently, this quantity could provide valuable information to try to identify the existence Fe species in Fe−Ni nanoparticles as bulk-like impurities, segregated on the surface, or forming core(Fe)−shell(Ni) structures.

D. Structural Properties and Magnetic Behavior of Polyicosahedral Fe−Ni Cluster Alloys. In this respect, it is also relevant to calculate the orbital-to-spin ratio for Fe−Ni cluster alloys having a polyicosahedral structure. This calculation is very interesting to perform because by means of gas-phase nitrogen adsorption experiments[5] it has been inferred that Fe impurities in these kind of clusters are also located, as predicted in this work for fcc nanoalloys, in the core region of the structures. It will be thus desirable to see if in these kind of atomic arrays, the orbital-to-spin ratio can be also used to corroborate the predicted internal location of the Fe impurities in Fe−Ni polyicosahedral cluster alloys. In Figure 11, we show the lowest energy atomic configurations obtained for polyicosahedral $FeNi_{25}$ and Fe_4Ni_{22} clusters with different chemical orders, together with their corresponding binding energies E_b and average spin moments calculated within the SIESTA methodology. In Figure 11a,c, we present the equilibrium structures found for a single Fe impurity and for 4 Fe atoms, respectively, occupying the core region of the structures, whereas in Figure 11b,d we show the lowest energy atomic configurations for one and four Fe atoms located on the surface of the particles. Similar to the fcc Fe−Ni clusters, our total energy calculations reveal that the location of the iron impurities in the central region of the structures is preferred (see Figure 11a,c), being more stable than the ones in which the iron surface segregation is assumed (by 0.45 eV between Figure 11a,b and by 1.7 eV between Figure 11c,d). It is important to remark that these energy differences are of the order of the ones obtained by Longo et al.[31] for similar Fe-dilute Fe−Ni polyicosahedral clusters of different sizes.

Finally, we have calculated by means of the tight binding model presented in Section II.B the local spin and orbital moment contributions to the total magnetization for the polyicosahedral single Fe-doped cluster alloys shown in Figure 11a,b. First it is important to remark that, as in the single Fe-doped fcc $FeNi_{42}$ cluster alloys, our calculated semiempirical average spin magnetization is also independent of the location of Fe atom in the structures, being equal to 0.9 μ_B /atom in both cases and very close also to the value obtained within the DFT approach, which is equal to 0.85μ_B/atom. In contrast, both the local spin $2S_z^{Fe}(i)$ and orbital $L_z^{Fe}(i)$ moments at the Fe atoms are found to be more sensitive to variations in the local atomic environment. In the core region (see Figure 11a), the Fe impurity is characterized by values of $2S_z^{Fe} = 2.28\mu_B$ and $L_z^{Fe} = 0.11\mu_B$, whereas on the surface (see Figure 11b) $2S_z^{Fe} = 2.79\mu_B$ and $L_z^{Fe} = 0.18\mu_B$. Of course, with this local magnetic moment contributions it is possible to calculate directly the orbital-to-spin ratio $L_z^{Fe}/2S_z^{Fe}$ for the two chemical configurations, and we obtain values of 0.048 and 0.064 for core and surface positions of the Fe atom, respectively. Clearly, as in the fcc Fe−Ni cluster alloys, the previous differences found for $L_z^{Fe}/2S_z^{Fe}$ in polyicosahedral Fe−Ni clusters will provide also a well-defined finger print to identify precise details of the chemical order within this kind of nanoalloys.

IV. Summary And Conclusions

In this work, we have performed both DFT (within the SIESTA method) and tight binding calculations to analyze the structural properties, chemical order, and magnetic behavior of fcc and polyicosahedral Fe−Ni cluster alloys. We have found that the total energy as well as the structural properties of our considered bimetallic alloys are highly dependent on the precise details of the chemical ordering within the particles. Interestingly, we have obtained that our Fe−Ni alloy clusters achieve their best stability when the iron atoms are located in the core region of the particles (in agreement with the experimental studies of Parks et al.) forming a compact structure, leading to the formation of highly stable core(Fe)−shell(Ni) chemical configurations. All our considered Fe−Ni clusters exhibit high-spin ground states (larger than the corresponding bulk alloy values for the same composition); however, we have found that iron clustering within the particles, the presence of atomic hydrogen chemisorbed on the surface, as well as the existence of antiferromagnetic order in the iron-reach regions could lead to a sizable quenching of the average magnetization in agreement with the experimental measurements of Li et al. Finally, we show that the value of the orbital-to-spin ratio in our Fe−Ni clusters is very sensitive to the internal location of the Fe impurities, a result that suggests that X-ray magnetic circular dichroism experiments can be very useful to reveal precise features of the chemical order in magnetic cluster alloys.

Acknowledgment. The authors would like to acknowledge the financial support from CONACyT through Grants 45928-F and 50650, as well as from PROMEP-SEP-CA. Finally, computer resources from Centro Nacional de Supercómputo (CNS) of the Instituto Potosino de Investigación Cientifica y Tecnológica (IPICyT), SLP, México, are also acknowledged.

References and Notes

(1) (a) Hong, R.; Fisher, N. O.; Emrick, T.; Rotello, V. M. *Chem. Mater.* **2005**, *17*, 4617. (b) Lee, W. R.; Kim, M. G.; Choi, J. R.; Park, J.; Koo, S. J.; Oh, S. J.; Cheon, J. *J. Am. Chem. Soc.* **2005**, *127*, 16090.

(2) (a) Shao, M. H.; Sasaki, K.; Adzic, R. R. *J. Am. Chem. Soc.* **2006**, *128*, 3526. (b) Tian, W. Q.; Ge, M.; Gu, F.; Yamada, T.; Aoki, Y. *J. Phys. Chem. A* **2006**, *110*, 6285. (c) Li, X. Q.; Zhang, W. X. *Langmuir* **2006**, *22*, 4638.

(3) (a) Crespo, P.; García, M. A.; Fernández Pinel, E.; Multigner, M.; Alcántara, D.; de la Fuente, J. M.; Penadés, S.; Hernando, A. *Phys. Rev. Lett.* **2006**, *97*, 177203. (b) Nguyen, H. L.; Howard, L. E. M.; Stinton, G. W.; Giblin, S. R.; Tanner, B. K.; Terry, I.; Hughes, A. K.; Ross, I. M.; Serres, A.; Evans, J. S. O. *Chem. Mater.* **2006**, *18*, 6414. (c) Ennas, G.; Falqui, A.; Paschina, G.; Marongiu, G. *Chem. Mater.* **2005**, *17*, 6486.

(4) (a) Gambardella, P.; Rusponi, S.; Veronese, M.; Deshi, S. S.; Grazioli, C.; Dallmeyer, A.; Cabria, I.; Zeller, R.; Dederichs, P. H.; Kern, K.; Carbone, C.; Brune, H. *Science* **2003**, *300*, 1130. (b) Jamneala, T.; Madhavan, V.; Crommie, M. F. *Phys. Rev. Lett.* **2001**, *87*, 256804. (c) Pick, S.; Stepanyuk, V. S.; Klavsyuk, A. L.; Niebergall, L.; Hergert, W.; Kirschner, J.; Bruno, P. *Phys. Rev. B* **2004**, *70*, 224419. (c) Heinrichs, S.; Dieterich, W.; Maass, P. *Phys. Rev. B* **2007**, *75*, 085437.

(5) Parks, E. K.; Kerns, K. P.; Riley, S. J. *Chem. Phys.* **2000**, *262*, 151.

(6) (a) Ferrando, R.; Fortunelli, A.; Rossi, G. *Phys. Rev. B* **2005**, *72*, 085449. (b) Guevara, J.; Llois, A. M.; Weissmann, M. *Phys. Rev. Lett.* **1998**, *81*, 5306.

(7) (a) Zitoun, D.; Respaud, M.; Fromen, M. C.; Casanove, M. J.; Lecante, P.; Amiens, C.; Chaudret, B. *Phys. Rev. Lett.* **2003**, *89*, 037203. (b) Antoniak, C.; Lindner, J.; Spasova, M.; Sudfeld, D.; Acet, M.; Farle, M.; Fauth, K.; Wiedwald, U.; Boyen, H.-G.; Ziemann, P.; Wilhelm, F.; Rogalev, A.; Sun, S. *Phys. Rev. Lett.* **2006**, *97*, 117201.

(8) (a) Guillaume, C. E. *C. R. Acad. Sci.* **1897**, *125*, 235. (b) Wasserman, E. F. In *Ferromagnetic Materials*; Buschow, K. H. J., Wohlfarth, E. P., Eds.; North-Holland: Amsterdam, 1990; Vol. 5, p 237.

(9) (a) Acet, M.; Wassermann, E. F.; Andersen, K.; Murani, A. and Schärpff, O. *J. Appl. Phys.* **1997**, *81*, 3876. (b) Zähres, H.; Acet, M.; Stam, W.; Wassermann, E. F. *J. Magn. Magn. Mater.* **1988**, *72*, 80.

(10) Lagarec, K.; Rancourt, D. G.; Bose, S. K.; Sanyal, B.; Dunlap, R. A. *J. Magn. Magn. Mater.* **2001**, *236*, 107.

(11) Sedov, V. L.; Tsigelnik, O. A. *J. Magn. Magn. Mater.* **1998**, *183*, 117.

(12) (a) Mauri, D.; Scholl, D.; Siegmann, H. C.; Kay, E. *Phys. Rev. Lett.* **1989**, *62*, 1900. (b) Lin, T.; Schwickert, M.; Tomaz, M. A.; Chen, H.; Harp, G. R. *Phys. Rev. B* **1999**, *59*, 13911. (c) Smirnova, E. A.; Abrikosov, I. A.; Johansson, B.; Vekilov, Y. K.; Baranov, A. N.; Stepanyuk, V. S.; Hegert, W.; Dederichs, P. H. *Phys. Rev. B* **1999**, *59*, 14417. (d) Cherifi, S.; Boeglin, C.; Stanescu, S.; Deville, J. P.; Mocuta, C.; Magnan, H.; Le Feevre, P.; Ohresser, P.; Brookes, N. B. *Phys. Rev. B* **2001**, *64*, 184405. (e) Schellenberg, R.; Meinert, H.; Perez, A.; Kisker, E. *Phys. Rev. B* **2001**, *64*, 104472.

(13) Li, X. G.; Chiba, A.; Takahashi, S. *J. Magn. Magn. Mater.* **1997**, *170*, 339.

(14) Guirado-López, R. A.; Desjonqueres, M. C.; Spanjaard, D. *Eur. Phys. J. B* **2005**, *36*, 67.

(15) Wende, H.; Scherz, A.; Wihelm, F.; Baberschke, K. *J. Phys.: Condens. Matter* **2003**, *15*, S547.

(16) Perdew, J. P.; Burke, K.; Ernzerhof, M. *Phys. Rev. Lett.* **1996**, *77*, 3865.

(17) Troullier, N.; Martins, J. L. *Phys. Rev. B* **1991**, *43*, 1993.

(18) Kleinman, L.; Bylander, D. M. *Phys. Rev. Lett.* **1982**, *48*, 1425.

(19) Soler, J. M.; Artacho, E.; Gale, J. D.; Garca, A.; Junquera, J.; Ordejoón, P.; Sánchez-Portal, D. *J. Phys.: Condens. Matter* **2002**, *14*, 2745.

(20) Castro, M.; Jamorsky, C. and Salahub, D. R. *Chem. Phys. Lett.* **1997**, *271*, 133.

(21) (a) Purdum, H.; Montano, P. A.; Shenoy, G. K.; Morrison, T. *Phys. Rev. B* **1982**, *25*, 4412. (b) Cox, D. M.; Trevor, D. J.; Whetten, R. L.; Rohlfing, E. A.; Kaldor, A. *Phys. Rev. B* **1985**, *32*, 7290. (c) Lin, S. S.; Kant, A. *J. Phys. Chem.* **1969**, *73*, 2450. (d) Shim, I.; Gingerich, K. A. *J. Chem. Phys.* **1982**, *77*, 2490. (e) Lian, L.; Su, C.-X.; Armentrout, P. B. *J. Chem. Phys.* **1992**, *97*, 4072.

(22) Ho, J.; Polak, M. L.; Ervin, K. M.; Lineberger, W. C. *J. Chem. Phys.* **1992**, *99*, 8542.

(23) Rollmann, G.; Entel, P.; Sahoo, S. *Comput. Mater. Science* **2006**, *35*, 275.

(24) Rao, B. K.; Ramos de Debiaggi, S.; Jena, P. *Phys. Rev. B* **2001**, *64*, 024418.

(25) Pastor, G. M.; Dorantes-Dávila, J.; Pick, S.; Dreyssé, H. *Phys. Rev. Lett.* **1995**, *75*, 326.

(26) Rodrguez-López, J. L.; Dorantes-Dávila, J.; Pastor, G. M. *Phys. Rev. B* **1998**, *57*, 1040.

(27) Félix-Medina, R.; Dorantes-Dávila, J.; Pastor, G. M. *Phys. Rev. B* **2003**, *67*, 094430.

(28) Friedel, J.; Lenglart, P.; Leman, G. *J. Phys. Chem. Solids* **1964**, *25*, 781.

(29) Bruno, P. *Magnetismus von Festkörpern und Grenzflächen*, Ferienkurse des Forschungszentrums Jülich; KFA: Jülich, Germany, 1993; Chapter 24.

(30) Haydock, R. In *Solid State Physics*; Ehrenreich, H., Seitz, G., Turnbull, D., Eds.; Academic: New York, 1980; Vol. 35, p 215.

(31) Longo, R. C.; Noya, E. G.; Gallego, L. J. *J. Chem. Phys.* **2005**, *122*, 084311.

(32) Guevara, J.; Llois, A. M.; Weissmann, M. *Phys. Rev. B* **1995**, *52*, 11509.

(33) Guirado-López, R. A.; Desjonqueres, M. C.; Spanjaard, D. *Phys. Rev. B* **2006**, *74*, 064415.

(34) Ducastelle, F. *Order and Phase Stability in Alloys*; de Boer, F. R., Petiffor, D. G., Eds.; North-Holland: Amsterdam, 1991.

(35) Tiago, M. L.; Zhou, Y.; Alemany, M. M. G.; Saad, Y.; Chelikowsky, J. R. *Phys. Rev. Lett.* **2006**, *97*, 147201.

(36) (a) Abrahams, S. C.; Guttman, L.; Kasper, J. S. *Phys. Rev.* **1962**, *127*, 2052. (b) Keune, W.; Halbauer, R.; Gonser, U.; Lauer, J.; Williamson, D. L. *J. Magn. Magn. Mater.* **1977**, *6*, 192. (c) Lee, K.; Callaway, J.; Kwong, K.; Tang, R.; Ziegler, A. *Phys. Rev. B* **1985**, *31*, 1796. (d) Dorantes-Dávila, J.; Dreyssé, H.; Pastor, G. M. *Phys. Rev. B* **1992**, *46*, 10432.

(37) (a) Hasegawa, M.; Batrashevich, M. I.; Zhao, T. R.; Takei, H. and Goto, T. *Phys. Rev. B* **2001**, *63*, 184437. (b) Meja-López, J.; Romero, A. H.; Garca, M. E.; Morán-López, J. L. *Phys. Rev. B* **2006**, *74*, 140405(R). Lounis, S.; Mavropoulos, P.; Zeller, R.; Dederichs, P. H.; Blügel, S. *Phys. Rev. B* **2007**, *75*, 174436.

(38) Hammer, L.; Landskron, H.; Nichtl-Pecher, W.; Fricke, A.; Heinz, K. ; Müller, K. *Phys. Rev. B* **1993**, *47*, 15969.

(39) Upton, T. H.; Goddard, W. A., III, *Phys. Rev. Lett.* **1979**, *42*, 472.

(40) (a) Le Cann, X.; Boeglin, C.; Carriére, B.; Hricovini, K. *Phys. Rev. B* **1996**, *54*, 373. (b) Vogel, J.; Fontaine, A.; Cross, V.; Petroff, F.; Kappler, J.-P.; Krill, G.; Rogalev, A.; Goulon, J. *Phys. Rev. B* **1997**, *55*, 3663. (c) Kamp, P.; Marty, A.; Gilles, B.; Hoffmann, R.; Marchesini S.; Belakhovsky, M.; Boeglin, C.; Dürr, H. A.; Dhesi, S. S.; van der Laan, G.; Rogalev, A. *Phys. Rev. B* **1999**, *59*, 1105.

(41) Heine, V. *Phys. Rev.* **1967**, *153*, 673.

(42) Moruzzi, V. L.; Marcus, P. M. In *Handbook of Magnetic Materials*; Buschow, K. H. J., Eds.; Elsevier, Science Publishers B.V.: New York, 1993; Vol. 7.

(43) Alvarado, P.; Dorantes-Dávila, J.; Pastor, G. M. *Phys. Rev. B* **1998**, *58*, 12216.

(44) Freyss, M.; Stoeffler, D.; Dreyssé, H. *Phys. Rev. B* **1997**, *56*, 6047.

(45) Victora, R. H.; Falicov, L. M.; Ishida, T. *Phys. Rev. B* **1984**, *30*, 3896.

(46) Pastor, G. M.; Dorantes-Dávila, J.; Bennemann, K. H. *Phys. Rev. B* **1989**, *40*, 7642.

(47) Stearns, M. B. In *3d, 4d, and 5d* Elements, Alloys, and Compounds; Wijn, H. P. J., Ed.; Springer-Verlag: Berlin, 1986; Group 3, Vol. 19, Part A.